Lech M. GRZESIAK[1], Bartłomiej UFNALSKI[1], Arkadiusz KASZEWSKI[1], Grzegorz GĄBKA[1], Paweł ROSZCZYK[2]

Warsaw University of Technology, Institute of Control and Industrial Electronics (1), Institute of Construction Machinery Engineering (2)

Power management in series hybrid drive

Streszczenie. *W artykule opisano układ laboratoryjny hybrydowego szeregowego zespołu napędowego dla pojazdu elektrycznego. Szczególną uwagę położono na metodę sterowania przekształtnikiem AC-DC współpracującym z zespołem silnik spalinowy-generator. Przedstawiono również dwie strategie sterowania silnikiem spalinowym oraz sposoby zarządzania rozdziałem mocy z dwóch źródeł energii w zależności od zapotrzebowania na moc przez silnik elektryczny. (**Zarządzanie rozdziałem mocy w hybrydowym napędzie szeregowym**).*

Abstract*. This paper presents an experimental setup of a series hybrid drive for an electric vehicle. The control method of AC-DC converter operating with engine-generator set is presented in detail. There have been presented two control strategies for internal combustion engine (ICE) and power management for two energy sources aimed at covering power demand of an electric motor.*

Słowa kluczowe: pojazd elektryczny, prostownik aktywny, napęd z maszyną PMSM.
Keywords: electric vehicle, active rectifier, PMSM motor drive.

Introduction

Hybrid electric vehicles (HEVs) are very promising alternatives to typical vehicles propelled by an internal combustion engine. There are many ways to create hybrid drives. Two major categories are parallel hybrids and series hybrids. In the parallel hybrid drive, electric motor and internal combustion engine are connected to mechanical transmission. In the series hybrid system, the ICE is not directly connected to the drivetrain, but propels generator. Energy produced by the engine-generator set and energy from the battery are summed in common DC circuit and passed to electric motor connected to the drivetrain. A generator output voltage is AC, thus an AC-DC converter must be applied to proper operation with electrochemical batteries. It is possible to reduce gases emission and fuel consumption in the hybrid drive by implementing control strategies that enable optimization of working point of the ICE. An electric machine can recuperate energy during breaking and charge the battery. Another advantage of series hybrid vehicle equipped with appropriately-sized battery storage is the possibility of pure electric drive in the city traffic.

Hybrid power system for EV

Proposed drive system consists of two energy sources: an internal combustion engine and an electrochemical battery. Power from both sources is summed in DC-link. A permanent magnet (PM) synchronous motor is supplied from DC-link via power electronic inverter. A block diagram of the system is depicted in fig.1.

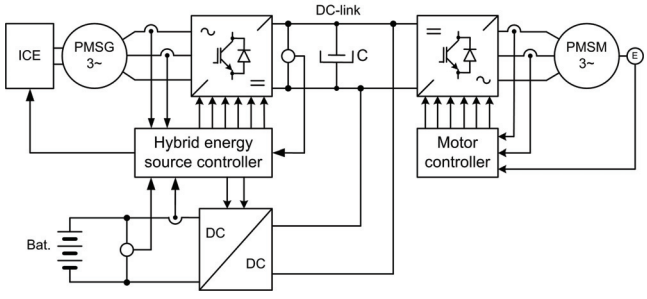

Fig.1. Series hybrid drive system.

The voltage converter operates with generator near unity power factor, and regulates DC voltage. The battery voltage is lower then DC-link voltage, therefore a step-up and step-down voltage converter was used. Controllers for all subsystems were developed on DSP platforms. CAN bus was used for communication between subsystems.

AC-DC converter

A typical diode rectifiers draw highly-distorted currents from generator, which are rich in harmonics with the order of 6k±1, that is, 5, 7, 11, 13, etc. These current harmonics result in lower power factor. A PWM rectifier has been applied to permanent magnet generator to overcome these drawbacks. Active rectifiers are often used in grid system applications to limit harmonic currents. One of the most popular control strategies for active rectifier is voltage oriented control (VOC) [1]-[3] in rotating coordinates aligned with measured line voltages. Another solution is based on the idea of direct power control (DPC) [4] without line voltage measurements. The idea of virtual flux is a background of the virtual flux oriented control (VFOC) [3],[5] and the virtual flux direct power control [6],[7].

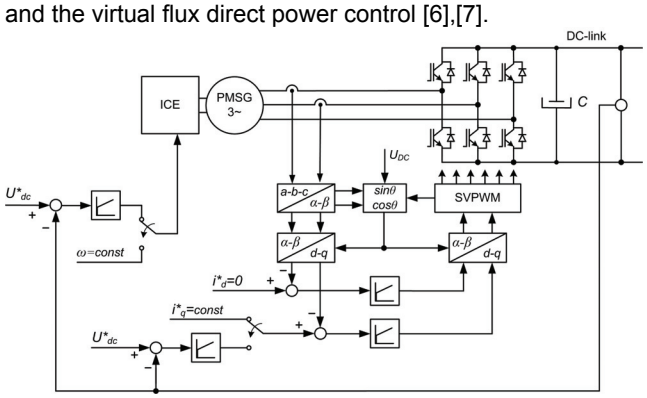

Fig.2. Active rectifier operating with ICE–generator set.

The aim of the control system is to draw nearly sinusoidal currents from the generator and maintain the output DC-link voltage at the required level. Control of the rectifier is based on calculations in a *d-q* frame oriented in such a way that the *d*-axis is aligned with the permanent magnet flux vector and *q*-axis is aligned with the generator electromotive force vector. The three-phase generator currents are transformed to rotating reference frame *d-q* by following transformation:

$$(1)\quad \begin{bmatrix} i_d \\ i_q \end{bmatrix} = \begin{bmatrix} \cos\theta & \frac{1}{\sqrt{3}}\sin\theta & -\frac{1}{\sqrt{3}}\sin\theta \\ -\sin\theta & \frac{1}{\sqrt{3}}\cos\theta & -\frac{1}{\sqrt{3}}\cos\theta \end{bmatrix} \begin{bmatrix} i_a \\ i_b \\ i_c \end{bmatrix}$$

In the synchronous rotating reference frame generator current components i_d and i_q become DC signals at steady-state conditions and they are used as a feedback signals for

controllers. The reference current *q*-component (i_q^*) is used to perform the DC voltage control and the reference current *d*-component (i_d^*) is controlled to obtain unity power factor. The output signals from current controllers are transformed from *d-q* frame to *α-β* stationary reference frame by transformation:

$$\begin{bmatrix} v_\alpha \\ v_\beta \end{bmatrix} = \begin{bmatrix} \cos\theta & -\sin\theta \\ \sin\theta & \cos\theta \end{bmatrix} \begin{bmatrix} v_d \\ v_q \end{bmatrix} \tag{2}$$

and then from *α-β* frame are transformed to natural coordinates *abc*:

$$\begin{bmatrix} v_a \\ v_b \\ v_c \end{bmatrix} = \begin{bmatrix} 1 & 0 \\ -1/2 & \sqrt{3}/2 \\ -1/2 & -\sqrt{3}/2 \end{bmatrix} \begin{bmatrix} v_\alpha \\ v_\beta \end{bmatrix} \tag{3}$$

Signals v_a, v_b, v_c are used for generating switching signals by space vector pulse width modulator (SVPWM) identical to modulator based on zero sequence signal [8].
Angle of rotating *d-q* frame is illustrated in the fig.3.

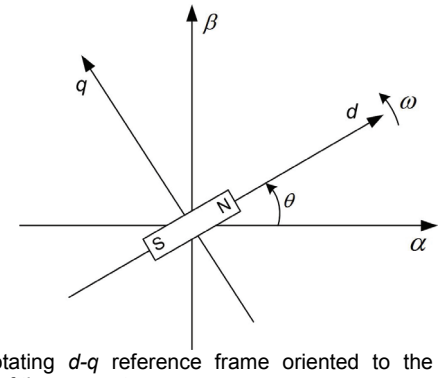

Fig.3. Rotating *d-q* reference frame oriented to the permanent magnets of the generator.

The generator voltage equation in stationary reference frame *α-β*:

$$\underline{u}_s = \frac{d\underline{\Psi}_s}{dt} - R_s \underline{i}_s \tag{4}$$

where: $\underline{u}_s$ – generator stator voltage vector, $\underline{\Psi}_s$ – generator stator flux vector, R_s – stator winding resistance, $\underline{i}_s$ - generator current vector,
is used for rotation angle determination.

Stator flux can be expressed by flux of permanent magnet and flux induced by stator current

$$\underline{\Psi}_s = \underline{\Psi}_{PM} - \underline{\Psi}_i \tag{5}$$

where:

$$\underline{\Psi}_i = L_s \underline{i}_s \tag{6}$$

Substituting (5) and (6) into (4), we obtain:

$$\underline{u}_s = \frac{d\underline{\Psi}_{PM}}{dt} - L_s \frac{d\underline{i}_s}{dt} - R_s \underline{i}_s \tag{7}$$

After rearranging (7), we get:

$$\frac{d\underline{\Psi}_{PM}}{dt} = L_s \frac{d\underline{i}_s}{dt} + \underline{u}_s + R_s \underline{i}_s \tag{8}$$

Integrating both sides of (8) gives:

$$\begin{cases} \Psi_{PM\alpha} = L_s i_{s\alpha} + \int (u_{s\alpha} + R_s i_{s\alpha})dt + \Psi_{PM\alpha}(0) \\ \Psi_{PM\beta} = L_s i_{s\beta} + \int (u_{s\beta} + R_s i_{s\beta})dt + \Psi_{PM\beta}(0) \end{cases} \tag{9}$$

Stator voltage components $u_{s\alpha}$ and $u_{s\beta}$ can be calculated from PWM duty cycles and DC-link voltage:

$$\begin{cases} u_{s\alpha} = 1/3 U_{dc}(2D_a - D_b - D_c) \\ u_{s\beta} = 1/\sqrt{3} U_{dc}(D_b - D_c) \end{cases} \tag{10}$$

where: D_a, D_b, D_c – duty cycles.
Finally we calculate operands used in transformations (1) and (2)

$$\begin{cases} \sin\theta = \Psi_{PM\beta} / \sqrt{\Psi_{PM\alpha}^2 + \Psi_{PM\beta}^2} \\ \cos\theta = \Psi_{PM\alpha} / \sqrt{\Psi_{PM\alpha}^2 + \Psi_{PM\beta}^2} \end{cases} \tag{11}$$

A practical implementation of (9) requires additional algorithms to cope with unknown initial conditions and DC-offsets introduced by measurement circuits. This problem can be solved by low-pass filtering implemented instead of a pure integration [9]. The practical solution to flux angle calculation problem is presented in the fig.4.

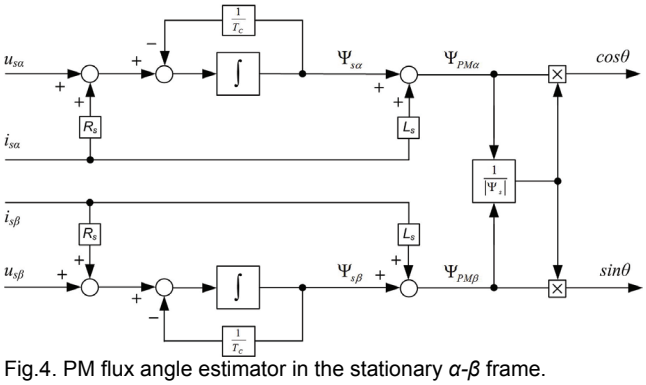

Fig.4. PM flux angle estimator in the stationary *α-β* frame.

DC-DC converter

The DC-link voltage is higher than the battery voltage, thus DC-DC converter shown in the fig.5 was applied for proper operation of the battery. The voltage converter is bidirectional and interfaces battery to the DC-link. The DC-DC converter operates in boost mode when the energy is delivered from the battery to the motor inverter. During regenerative braking of the vehicle or when the power delivered by engine-generator set is higher than the load power the DC-DC converter charges the battery in step-down mode.

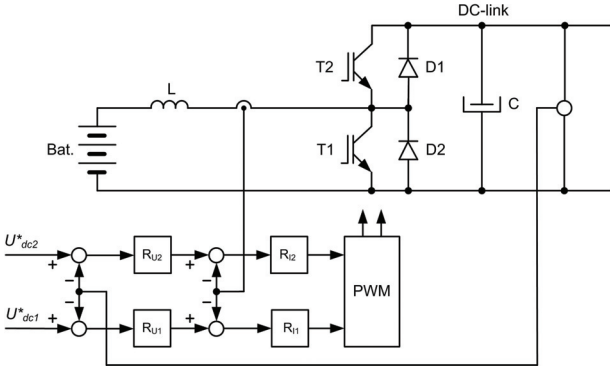

Fig.5. The bi-directional DC-DC converter.

There are two control loops: inner loop regulates current and outer loop maintains DC-link voltage at the required level. Voltage levels for control system of the hybrid energy source are depicted in the fig.6. There are two different levels of reference DC voltage for battery chopper: U^*_{dc1} is reference voltage for step-up mode and U^*_{dc2} is reference voltage for step-down mode. A reference voltage for the AC-DC converter is set in the middle of these two levels. Relations between three reference voltage levels defined

within control system of discussed hybrid energy source are depicted in fig.6. No current flows between battery and DC-link when the load power is balanced by the engine-generator set.

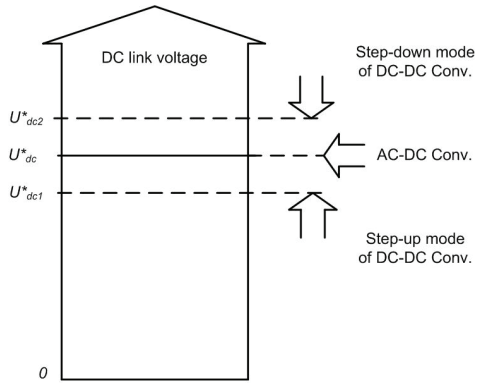

Fig.6. Reference voltage levels for the converters.

Any effective battery management system requires a state of charge (SOC) estimation. A method based on nonlinear dynamics modeling [10] can be used for determining SOC. Based on experimental data from charging and discharging battery it is possible to describe electromotive force (EMF) and internal resistance as a function of SOC by following polynomials:

$$E(k) = A_e k^6 + B_e k^5 + C_e k^4 + D_e k^3 + E_e k^2 + F_e k + G_e$$
$$R_w(k) = A_r k^6 + B_r k^5 + C_r k^4 + D_r k^3 + E_r k^2 + F_r k + G_r \quad (12)$$

where k denotes SOC and $0 \le k \le 1$.

The following equation is the background to determine accurate value of SOC for dynamic conditions [11]:

$$u(t) = E(k) \pm R_w(k) i(t) \quad (13)$$

where: $u(t)$, $i(t)$ – battery voltage and current, $E(k)$, $R_w(k)$ - polynomials (12) for real battery module.

Based on equation (13), the SOC can be obtained by look-up table or bisection iterative method.

Control strategies

The ICE should work within the area of the lowest fuel consumption. There have been considered two control strategies for combustion engine propelling the generator. The first one assumes that the engine works with constant speed and variable torque as depicted in the fig.7a. In the second strategy the engine operates with variable speed and constant torque as shown in the fig.7b.

In the first concept torque can increase in relatively very short time, because it depends on the throttle time constant. This means that power response of the engine-generator set is very fast. In the second case speed can increase according to the equation:

$$\frac{d\omega}{dt} = \frac{1}{J} T_d = \frac{1}{J}(T_m - T_l) \quad (14)$$

where: ω – engine speed, J – total inertia of the engine-generator set, T_m – engine maximum torque, T_l – load torque.

Time constant of the mechanical system is significantly bigger, thus the acceleration of the ICE is relatively slow and power response of the engine-generator set is slower in comparison to the first strategy.

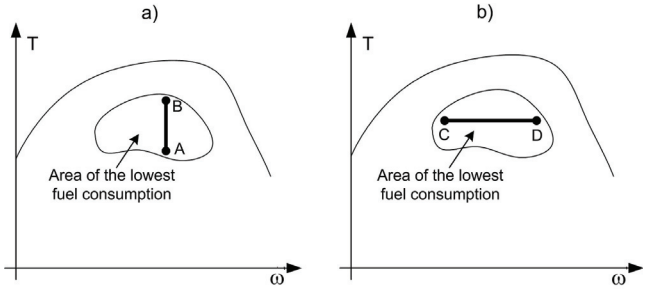

Fig.7. Concepts of the engine control: a) constant speed, b) constant torque.

Battery state of charge (SOC) is used for selecting control strategy of the engine generator set. The internal resistance of installed gel lead-acid battery as a function of SOC is shown in the fig.8. There are three regions distinguished by internal resistance behavior versus SOC. The battery has the lowest internal resistance in the middle region and should be operated in this region to limit the energy losses during charging and discharging. Battery capacity should be minimized to reduce its mass and cost. The design must take into account that it is difficult to keep SOC of low-capacity battery in the boundary that guarantees the lowest internal resistance and at the same time to operate engine in the area of the lowest fuel consumption. The control of the system must minimize time operation of the battery in overcharge and overdischarge states [12],[13].

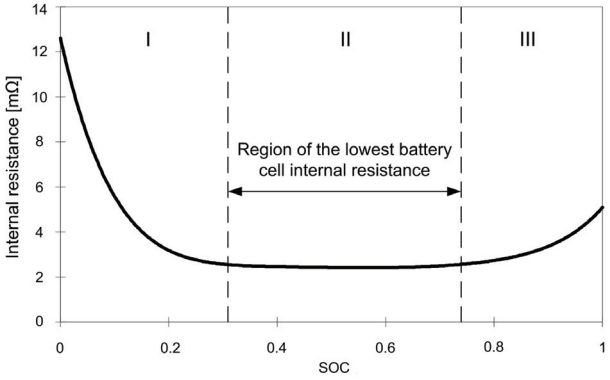

Fig.8. Internal resistance versus SOC.

In the first region when SOC is approaching zero, internal resistance of the battery is increasing rapidly. Engine operates with variable torque at constant speed. This control strategy allows to avoid discharging battery during transients of the engine-generator set. The speed of ICE is stabilized by a built-in controller. Torque on engine shaft is equal to generator electromagnetic torque (15) summed with friction torque.

$$T_e = \frac{3}{2} p \Psi_{PM} i_q \quad (15)$$

The engine load torque is determined by the generator current i_q. The reference value of generator q-component current is provided by a voltage regulator which stabilizes DC-link voltage on the level of U^*_{dc}. The relationship between the DC-link voltage, the generator current and the battery current is shown in the fig.9a. The DC-DC converter starts pumping current from the battery when DC-link voltage drops below U^*_{dc1} level. Power distribution for this strategy is depicted in the fig.9b. This strategy provides fast generator power response to motor power demand. Battery is not discharged during transients but only in steady states when desired power is higher than generator power in

operating point B (see fig.7). If the load power is lower than generator power in operating point A then excessive energy is pumped into the battery.

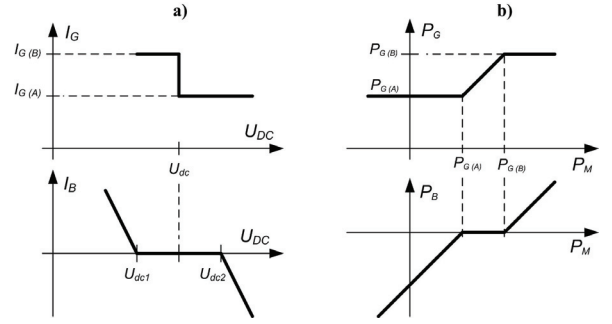

Fig.9. Control strategy in the I region: a) relationship between DC-link voltage, generator current and battery current, b) power distribution of the generator and the battery vs. motor power.

The second region (see fig.8) is optimal for battery discharging and charging. The engine operates with constant torque and variable speed. The battery supports engine-generator set during acceleration of ICE to give fast power response. This strategy is characterized by slow power response of the generator but power can be varied in the wider range across the area of the lowest fuel consumption.

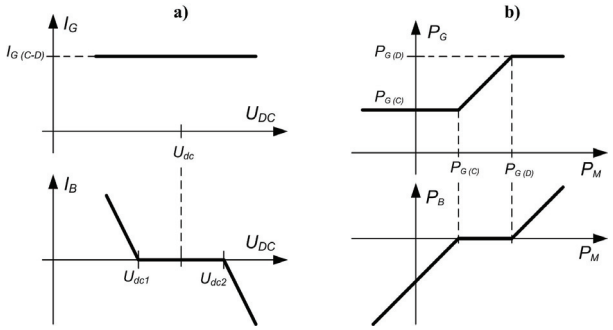

Fig.10. Control strategy in the II region: a) relationship between DC-link voltage, generator current and battery current, b) power distribution between the generator and the battery vs. motor power.

The constant torque mode of operation for the engine is achieved by keeping generator current at constant level. Desired speed is evaluated by a DC-link voltage regulator. If motor load increases then a DC-link capacitor voltage drops and the controller increases a reference speed signal for the ICE until power balance is met in the system. Power of the generator is expressed by equation:

$$P_G = \frac{3}{2} p \Psi_{PM} i_q \omega_{ICE} \tag{16}$$

Power delivered by the generator is proportional to ICE angular speed in constant current (torque) mode.

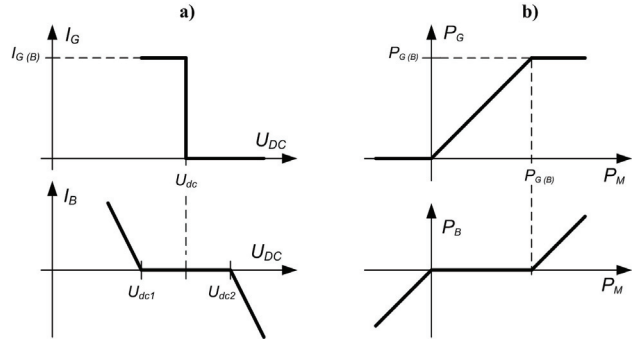

Fig.11. Control strategy in the III region: a) relationship between DC-link voltage, generator current and battery current, b) power distribution between the generator and the battery vs. motor power.

Within the third region (see fig.8) battery should be charged only during recuperative braking to avoid overcharging. The engine operates with variable torque at constant speed. On the contrary to control strategy in the first region, engine torque can vary not only in the area of the lowest fuel consumption but can be reduced below operating point A if the motor load power is lower than the generator power in this operating point. As it is shown in the fig.11 generator power is varied from zero to $P_G(B)$ in operating point B.

Experimental test results

A laboratory setup of hybrid series drive system has been developed for control strategies testing purposes. The stand for the tests is shown in the fig.12. The single-leg IGBT modules were used to build power electronic converters. Three DSP platforms were applied to implement control algorithms for the AC-DC converter, the inverter for motor, and the DC-DC converter.

Fig.12. Experimental setup.

All subsystems are governed by the master controller. It is possible to connect external device via CAN bus to collect data from the system, to change selected settings, or to establish new source of reference signals like braking torque or speed of the vehicle.

Tab.1. Parameters of the experimental hybrid series drive system

Engine: 4 stroke petrol engine, single-cylinder		
Displacement [cm^3]	438	
Power [kW] @ 3600 rpm	9.5	
Max. torque [Nm] @ 2500 rpm	29.8	
Reduced torque of inertia [kgm^2]	0.12	
PM machines	generator	motor
Nominal power [kW]	15	15
Nominal speed [rpm]	3600	3600
Nominal voltage [V]	224	229
Nominal current [A]	44	43
Reduced torque of inertia [kgm^2]	0.036	6
Battery: gel lead-acid		
Voltage [V]	144	
Capacity [Ah]	77	
Power electronics converters		
DC link voltage [V]	300	
Switching frequency [kHz]	10	

Dynamics of the vehicle is reproduced by a rotating mass attached to the shaft. Driving cycle profiles have been defined and implemented for various test scenarios. They include common states of a vehicle: acceleration, constant speed, recuperative braking and vehicle stoppage. The variable-speed and constant-torque operation mode for the ICE has been realized by drawing constant current from generator. As it is shown in fig. 13 and 14, the speed of ICE is growing during acceleration of the drive. The battery supports the engine-generator set in dynamic states. During no-load states battery is charged by the generator.

The constant-speed and variable-torque operation mode for the ICE has been realized by setting constant reference speed for the engine's built-in governor and by regulating generator current. Test results for operation mode in the third region (see fig.8) are illustrated in the fig. 15 and 16.

The battery is charged only during recuperative breaking of the vehicle.

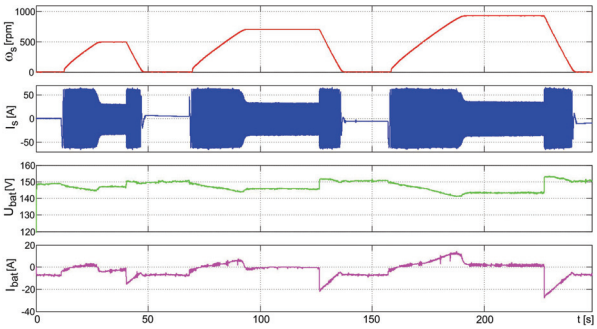

Fig.13. Experimental results for constant torque and variable speed mode of ICE: motor speed, motor current, battery voltage, battery current.

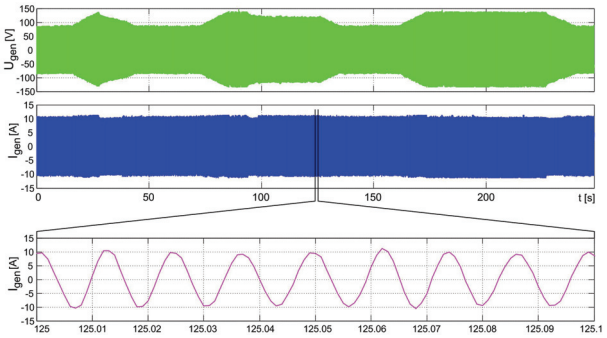

Fig.14. Experimental results for constant torque and variable speed mode of ICE: generator voltage, generator current.

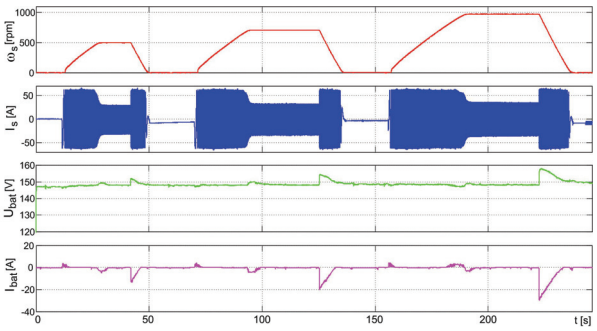

Fig.15. Experimental results for variable torque and constant speed mode of ICE: motor speed, motor current, battery voltage, battery current.

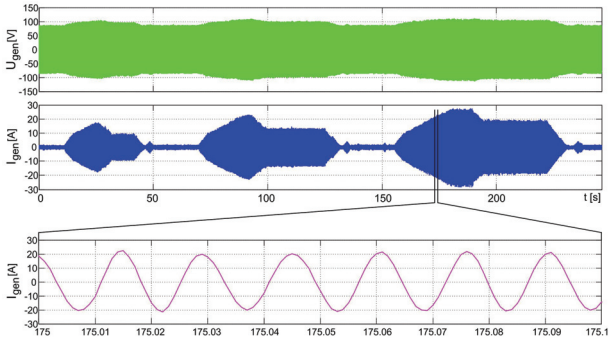

Fig.16. Experimental results for variable torque and constant speed mode of ICE: generator voltage, generator current.

Conclusions

Power electronic converters for a permanent magnet generator and an electrochemical battery dedicated to a series HEV powertrain have been tested experimentally in a laboratory environment. Two ICE operation modes have been implemented and tested. Electrochemical battery operating regions have been defined and recommendation for ICE control strategy in each SOC region has been made. It was shown how series hybrid electric drivetrain can deliver demanded power in transient and steady states of the vehicle taking also into account fuel consumption optimization.

The work was supported by the Ministry of Science and Higher Education (Poland) in the frame of the project No. R03 034 01.

REFERENCES

[1] Zeng, Q.; Chang, L.; Song, P., SVPWM-based current controller with grid harmonic compensation for three-phase grid-connected VSI, *Power Electronics Specialists Conference, 2004. PESC 04. 2004 IEEE 35th Annual*, (2004), n.4, 2494 - 2500

[2] Liserre, M.; Dell'Aquila, A.; Blaabjerg, F., An overview of three-phase voltage source active rectifiers interfacing the utility, *Power Tech Conference Proceedings, 2003 IEEE Bologna*, (2003), n.3

[3] Malinowski, M.; Kazmierkowski, M.P., Trzynadlowski, A.M., A comparative study of control techniques for PWM rectifiers in AC adjustable speed drives, *IEEE Transactions on Power Electronics*, 18 (2003), n.6, 1390 – 1396

[4] Noguchi, T., Tomiki, H., Kondo, S., Takahashi, I., Direct power control of PWM converter without power-source voltage sensors, *IEEE Transactions on Industry Applications*, 34 (1998) n.3, 473 – 479

[5] Duarte, J.L.; Van Zwam, A.; Wijnands, C.; Vandenput, A., Reference frames fit for controlling PWM rectifiers, IEEE Transactions on Industrial Electronics, 46 (1999), n.3, 628 - 630

[6] Malinowski, M.; Jasinski, M.; Kazmierkowski, M.P., Simple direct power control of three-phase PWM rectifier using space-vector modulation (DPC-SVM), *IEEE Transactions on Industrial Electronics,* 51 (2004), n.2, 447 - 454

[7] Malinowski, M.; Kazmierkowski, M.P., Hansen, S.; Blaabjerg, F.; Marques, G.D., Virtual-flux-based direct power control of three-phase PWM rectifiers, *IEEE Transactions on Industry Applications,* 37 (2001), n.4, 1019 – 1027

[8] Grzesiak, L.M., Ufnalski, B., Kaszewski, A., An Efficient Discontinuous Pulse Width Modulation Algorithm for Multileg Voltage-Source Converters, *Proceedings of the 2011 IEEE International Symposium on Industrial Electronics*

[9] B.Ufnalski, L.M.Grzesiak., Selected methods in flux estimation for induction motor drives, chapter in monograph Power electronics and electrical drives - selected problems, *edited by T.Orlowska-Kowalska,* Wroclaw 2007

[10] Szumanowski, A., Yuhua Chang, Battery Management System Based on Battery Nonlinear Dynamics Modeling, *IEEE Transactions on Vehicular Technology*, 57 (2008), n.3, 1425 – 1432

[11] Szumanowski, A., Nonlinear Dynamics: Nonlinear Dynamics Traction Battery Modeling, *edited by Todd Evans*, (2010), 199 – 220

[12] Hajduga, A., Szumanowski, A., Roszczyk, P., Dobór zespołu silnik spalinowy–generator w napędzie Plug-in hybryd lekkiego samochodu miejskiego. *XX Konferencja naukowa Problemy Rozwoju Maszyn Roboczych*, Zakopane 2007.

[13] Szumanowski, A., Hybrid Electric Vehicle Drives Design edition based on urban buses, *Monograph Book*, Warsaw-Radom 2006

***Authors**: dr hab. inż. Lech M. Grzesiak, prof. nzw., E-mail: lech.grzesiak@ee.pw.edu.pl; dr inż. Bartłomiej Ufnalski, E-mail: bartlomiej.ufnalski@ee.pw.edu.pl; mgr inż. Arkadiusz Kaszewski, E-mail: arkadiusz.kaszewski@ee.pw.edu.pl; mgr inż. Grzegorz Gąbka, Politechnika Warszawska, Instytut Sterowania i Elektroniki Przemysłowej, ul. Koszykowa 75, 00-662 Warszawa, E-mail: grzegorz.gabka@ee.pw.edu.pl; mgr inż. Paweł Roszczyk, Politechnika Warszawska, Instytut Maszyn Roboczych Ciężkich, ul. Narbutta 84, 02-524 Warszawa, E-mail: pawel.roszczyk@simr.pw.edu.pl.*